Mon. Not. R. Astron. Soc. **000**, 1–10 (0000) Printed 10 June 2015 (MN LATEX style file v2.2)

Limits on Fast Radio Bursts at 145 MHz with ARTEMIS, a real-time software backend

A. Karastergiou[1,2,3], J. Chennamangalam[1], W. Armour[4], C. Williams[1], B. Mort[4], F. Dulwich[4], S. Salvini[4], A. Magro[5], S. Roberts[6], M. Serylak[3], A. Doo[7], A. V. Bilous[8], R. P. Breton[9], H. Falcke[8,10], J.-M. Grießmeier[11,12], J. W. T. Hessels[10,13], E. F. Keane[14], V. I. Kondratiev[10,15] M. Kramer[16], J. van Leeuwen[10,13], A. Noutsos[16], S. Osłowski[16,17], C. Sobey[10], B. W. Stappers[9], P. Weltevrede[9],

[1] *Astrophysics, University of Oxford, Denys Wilkinson Building, Keble Road, Oxford OX1 3RH, UK*
[2] *Department of Physics and Electronics, Rhodes University, PO Box 94, Grahamstown 6140, South Africa*
[3] *Physics Department, University of the Western Cape, Cape Town 7535, South Africa*
[4] *Oxford e-Research Centre, University of Oxford, Keble Road, OX1 3QG, United Kingdom*
[5] *Institute of Space Sciences and Astronomy, University of Malta, Msida. MSD2080. Malta*
[6] *Information Engineering,University of Oxford, Oxford OX1 3PJ, UK*
[7] *STFC Chilbolton Observatory*
[8] *Department of Astrophysics/IMAPP, Radboud University Nijmegen, PO Box 9010, 6500 GL Nijmegen, The Netherlands*
[9] *Jodrell Bank Centre for Astrophysics, School of Physics and Astronomy, The University of Manchester, Manchester M13 9PL, UK*
[10] *ASTRON, The Netherlands Institute for Radio Astronomy, Postbus 2, 7990 AA Dwingeloo, The Netherlands*
[11] *LPC2E - Université d'Orléans/CNRS*
[12] *Station de Radioastronomie de Nançay, Observatoire de Paris - CNRS/INSU, USR 704 - Univ. Orleans, OSUC, 18330 Nançay, France*
[13] *Anton Pannekoek Institute for Astronomy, University of Amsterdam, Postbus 94249, 1090 GE Amsterdam, The Netherlands*
[14] *SKA Organisation, Jodrell Bank Observatory, Lower Withington, Macclesfield, Cheshire, SK11 9DL, UK*
[15] *Astro Space Centre, Lebedev Physical Institute, Russian Academy of Sciences, Profsoyuznaya Str. 84/32, Moscow 117997, Russia*
[16] *Max-Planck-Institut für Radioastronomie, Auf dem Hügel 69, 53121 Bonn, Germany*
[17] *Fakultät für Physik, Universität Bielefeld, Postfach 100131, D-33501, Bielefeld, Germany*

10 June 2015

ABSTRACT

Fast Radio Bursts (FRBs), are millisecond radio signals that exhibit dispersion larger than what the Galactic electron density can account for. We have conducted a 1446 hour survey for Fast Radio Bursts (FRBs) at 145 MHz, covering a total of 4193 sq. deg on the sky. We used the UK station of the LOFAR radio telescope – the Rawlings Array – , accompanied for a majority of the time by the LOFAR station at Nançay, observing the same fields at the same frequency. Our real-time search backend, ARTEMIS, utilizes graphics processing units to search for pulses with dispersion measures up to 320 cm^{-3} pc. Previous derived FRB rates from surveys around 1.4 GHz, and favoured FRB interpretations, motivated this survey, despite all previous detections occurring at higher dispersion measures. We detected no new FRBs above a signal-to-noise threshold of 10, leading to the most stringent upper limit yet on the FRB event rate at these frequencies: 29 sky^{-1} day^{-1} for 5 ms-duration pulses above 62 Jy. The non-detection could be due to scatter-broadening, limitations on the volume and time searched, or the shape of FRB flux density spectra. Assuming the latter and that FRBs are standard candles, the non-detection is compatible with the published FRB sky rate, if their spectra follow a power law with frequency ($\propto \nu^{\alpha}$), with $\alpha \gtrsim +0.1$, demonstrating a marked difference from pulsar spectra. Our results suggest that surveys at higher frequencies, including the low frequency component of the Square Kilometre Array, will have better chances to detect, estimate rates and understand the origin and properties of FRBs.

Key words: instrumentation: miscellaneous — pulsars: general

1 INTRODUCTION

High-time resolution radio astronomy is entering a new era due to two developments. Firstly, new radio telescopes are being built that combine very high instantaneous sensitivity with wide fields of view, as required for blind searches of short duration events of transient radio emission. Secondly, high performance computing (HPC) enables us to process the data extremely quickly, providing the opportunity to discover and react to such events, enabling localization and classification.

Our quest to explore the dynamic nature of the radio sky is underpinned by the realization that bright, short duration radio bursts must originate from extreme physical processes taking place around compact sources. Neutron stars offer prime examples of such phenomena, being reliable emitters of short duration (typically 50 ms or less) radio pulses (Lorimer & Kramer 2005). These signals are observed once per rotational period for the majority of ordinary pulsars, but can be as infrequent as a few pulses per day in the case of Rotating Radio Transients (RRATS; McLaughlin et al. 2006). In addition to neutron stars, a new class of extraordinary sources has been identified in high time resolution radio astronomy which highlights the importance of real-time processing. The first of these sources – that have now come to be known as Fast Radio Bursts (FRBs) – was discovered by Lorimer et al. (2007), who reported the detection of a burst using the Parkes radio-telescope, with evidence supporting large, extragalactic distance. Following this discovery, more such bursts have been detected (Keane et al. 2012; Thornton et al. 2013; Spitler et al. 2014; Burke-Spolaor & Bannister 2014; Petroff et al. 2015; Ravi, Shannon, & Jameson 2015). We stress that all these events except Petroff et al. (2015) were discovered via offline processing of recorded data, therefore no immediate follow-up observations to localize them were possible. The origin of FRBs is unclear. Proposed explanations include flaring magnetars (Popov & Postnov 2013), binary neutron star mergers (Totani 2013), gravitational collapse of neutron stars to black holes (Falcke & Rezzolla 2014), emissions from companions of extragalactic pulsars (Mottez & Zarka 2014), and at least one Galactic proposition in the form of nearby flare stars (Loeb et al. 2014). These associations can be strengthened or weakened by comparing the rates of these events to the observed rates of FRBs. Current best limits from the observed FRBs are given by Thornton et al. (2013) as 10^4 sky^{-1} day^{-1}, or a volumetric rate of 10^{-3} gal^{-1} year^{-1}.

In general, an FRB will be dispersed by the free electron content of the medium it propagates through. As a result, the lower frequency components of a broadband burst arrive later than their high frequency counterparts, the delay at a given frequency ν being proportional to the line integral of the electron column density along the line of sight (known as the dispersion measure) and ν^{-2}. There is some evidence that the dispersion measure (DM) of one of the aforementioned FRBs – the Keane et al. (2012) burst – may be explained by the Galactic distribution of electrons (Bannister & Madsen 2014). If FRBs are indeed extragalactic in origin, they can be used to quantify the ionized matter in the intergalactic medium (IGM), thereby allowing us to determine the baryon content of the universe. This could help solve the long-standing 'missing baryon problem' in cosmology, where there is a discrepancy between the observed and the expected quantities of baryons (Persic & Salucci 1992; McQuinn 2014). Answering this question is one of the science objectives of the Square Kilometre Array (SKA Macquart et al. 2015).

There is an expectation that astrophysical bursts will emit across a broad range of radio frequencies. The observed signal-to-noise ratio of an FRB can be maximized by correcting for the dispersion induced delays across the frequency band of a telescope, in a well established process from pulsar astronomy called dedispersion. In the specific context of a blind search for FRBs, where the DM is not known, the main challenge is to perform the incoherent dedispersion transform on the data. By this, we mean the process of producing from time series of total power in a large number of narrow frequency channels, time series of total power over a large range of DM values, revealing potential FRB candidates. This is a computationally expensive task, and performing it in real time requires specialized software running on high performance computers with accelerated hardware. In the last few years, implementations of the accelerated dedispersion transform that are capable of real-time processing of typical data streams have emerged (Armour et al. 2012; Barsdell et al. 2012; Magro et al. 2011) and are gradually being applied to surveys.

Comprehensive arguments in favour of searching for individual bright and dispersed pulses have been present in the literature and applied in practice for many years (see, for example, McLaughlin & Cordes 2003). Yet despite the discoveries mentioned above, we are still in the early stages of putting together a complete picture of the dynamic nature of the radio sky. The most up-to-date limits hitherto on fast transient sources at 150 MHz can be found in Coenen et al. (2014), who use the results of the LOFAR Pilot Pulsar Survey (LPPS) to derive an upper limit on the FRB rate of 150 sky^{-1} day^{-1}. All aforementioned FRBs have been discovered at a frequency around 1400 MHz. Upper limits to the FRB rate at different frequencies provide constraints on the luminosity distribution and the spectral characteristics. Assuming the flux density spectra of FRBs follow a power law, then

$$S(\nu) \propto \nu^{\alpha}, \tag{1}$$

where $S(\nu)$ is the flux density of the burst as a function of frequency ν, α is the spectral index. Low frequency FRB surveys are also being carried out at the Murchison Widefield Array (MWA), a low frequency dipole array located in Western Australia operating between 80 and 300 MHz. Trott, Tingay, & Wayth (2013) suggest several expected FRBs per observing week, providing a clear framework for estimating FRB rates depending on their intrinsic spectral index and scattering properties. There is currently no published detection of an FRB from the MWA in the literature.

The Low Frequency Array, LOFAR, is currently the most sensitive radio telescope in the world at frequencies between 30 and 250 MHz. It is a prototypical example of a 'next-generation radio telescope' and a pathfinder towards the Square Kilometre Array (SKA). The telescope is described in detail in van Haarlem et al. (2013). Discovery of pulsars and fast transients is one of the key science goals of LOFAR, as outlined in Stappers et al. (2011). We present here details and first results of a programme to use one inter-

national LOFAR station to search for FRBs, in an effort to characterize the dynamic nature of the radio sky at LOFAR frequencies. In this paper, we describe the system developed to conduct fast transient surveys and the results of the first survey.

This paper is organized as follows. In §2, we describe the project, including details of the hardware and software, and the signal processing algorithms, and in §3, we describe our survey for fast transients using ARTEMIS, before concluding in §4.

2 THE ARTEMIS PROJECT

We have put together the hardware and software that is required to continuously monitor the large LOFAR fields of view and detect FRBs in real time using general purpose computing on graphics processing units (GPUs). The scientific potential and the technical challenge of real-time FRB discovery were the prime motivating factors behind the Advanced Radio Transient Event Monitor and Identification System (ARTEMIS) project, with an emphasis on applying HPC techniques to data from next generation telescopes. The primary goals of the ARTEMIS project therefore consist of:

- Enabling the science goals of the SKA and its pathfinders in the area of surveys for new pulsars and exotic fast transients.
- Exploiting many-core technologies to minimize capital costs of hardware, whilst delivering energy-efficient solutions for streaming processing in radio astronomy.

2.1 Technical description

We use the high-band antennas (HBA) of a single international LOFAR station, which consists of 96 dual-polarization antennas covering a frequency range between 110 and 250 MHz. The ARTEMIS installation currently uses four 12-core servers, each equipped with a single Fermi NVIDIA GPU card located on site at the Rawlings Array in the UK (a similar setup exists at the international LOFAR station in Nançay, France and an ARTEMIS server for offline pulsar data processing exists in Jülich, Germany). The servers receive data through a broadband (10 Gbps) switch, which is also responsible for sending the data back to the LOFAR correlator in the Netherlands, for normal operations of the International LOFAR Telescope (ILT). Each LOFAR station generates a total of 3.2 Gbps of beamformed data, which corresponds to a sky bandwidth of approximately 48 MHz using 16-bit sampling. The station beamformer produces a total of 244 beamlets each with the frequency and time resolution specified in Table 1. Estimated values of the system equivalent noise are also given, for an observation with a total bandwidth of 6 MHz and time resolution of 327.68 μs, by scaling the sensitivity values, as given in Table B.3. of van Haarlem et al. (2013) for a source at 30°declination, to the aforementioned bandwidth and sample time. The sensitivity value quoted for 150 MHz is in good agreement with the value from the LPPS survey (Coenen et al. 2014) using uncalibrated LOFAR stations, scaled to this survey.

For this survey, groups of 30 and 31 beamlets are pointed in a single direction on the sky, covering contiguous frequency channels to form a total of 8 broadband ($\sim$ 6 MHz) beams. These can be formed within a circle of $\sim$10 times the beamlet FWHM, due to the analog tile beamforming of LOFAR HBA arrays described in Stappers et al. (2011).

Each ARTEMIS server receives and processes 2 out of the 8 formed beams, corresponding to a quarter of the total bandwidth. In addition to FRB detection, real-time processing can be used to reduce the data rate from 400 MB/s to manageable rates both for storage and further processing, useful for other science goals.

Table 1. Specifications of an international LOFAR station

Frequency (MHz)	Beamlet FWHM (deg)	Sensitivity (Jy, $\Delta\nu$=6 MHz, δt=327.68 μs)
30	9.9	1566
60	4.0	1079
120	2.5	33
150	2	27

Elevation range:	30° to 90°
Maximum number of beamlets:	244
Maximum total sky bandwidth:	47.65625 MHz
Sampling rate:	200 or 160 Msamples/s
Beamlet frequency resolution:	195.3125 or 156.25 kHz
Beamlet time resolution:	5.12 or 6.4 μs

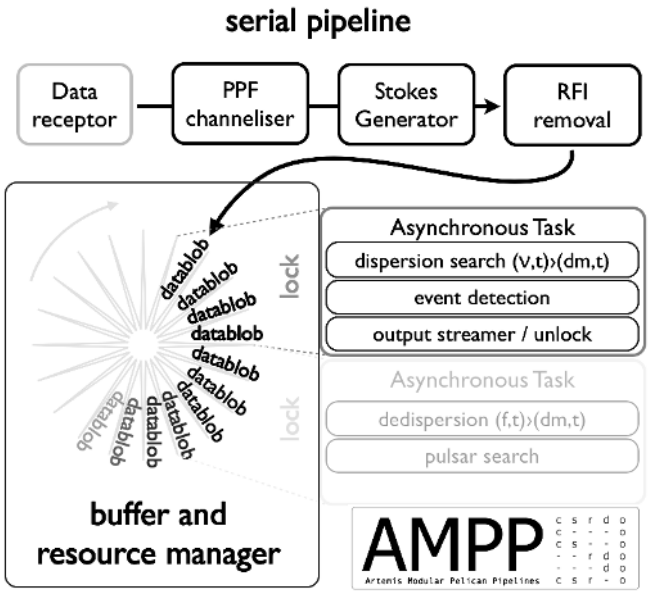

Figure 1. A block diagram of the ARTEMIS software, outlining the main processing modules, buffers and asynchronous tasks.

2.2 Software overview and framework

ARTEMIS provides an extendible and parallelisable software backend, which can process telescope data in real time, mainly for detecting FRBs. The software, called AMPP, is sufficiently generic to serve as an all-purpose telescope backend, which is built upon a C++ framework (PELI-

CAN[1]), providing a fully configurable client-server architecture. The software pipelines consist of a number of C++ modules and configuration files for processing live telescope data. The modular design allows data processing tasks to be implemented independently of other considerations such as data acquisition, transport protocols, data output, and system deployment. The modules currently available include an implementation of a polyphase filter for raw (coherent) telescope data, a Stokes-generating and integration module which converts the raw data to Stokes parameters, a radio-frequency interference (RFI, unwanted and often man-made signals) rejection module which operates on incoherent data, an incoherent dedispersion transform module, and streaming modules that record data to disk and send the processed data via the network for further processing or recording. Figure 1 shows a schematic of AMPP. As shown, dedispersion is an asynchronous task which occurs only when sufficient data have been accumulated in a buffer. This task is also the most expensive in terms of computation, and therefore is accelerated using GPUs. AMPP uses the AstroAccelerate dedispersion transform algorithm (Armour et al. 2012), which has been favourably benchmarked against other extremely fast implementations (Barsdell et al. 2012; Magro et al. 2011).

2.3 Spectral processing and RFI excision

In aperture arrays such as LOFAR, beamforming can require that spectral channels are formed in the raw digital data (Mol & Romein 2011). This is achieved prior to beamforming via a polyphase filter followed by a fast Fourier transform, which produces a number of raw-data frequency subbands. The channelisation requirements of the beamformer are generally different to those of the dedispersion transform, therefore an additional channelisation step is necessary within the software. Incoherent dedispersion cannot remove intra-channel dispersion. As a result, the channel bandwidth should not exceed a certain limit, dictated by the maximum DM of a search and the minimum duration of the FRBs being searched for. Determining this limit is standard practice in pulsar and fast transient searches (e.g., Keith et al. 2010).

We have developed a multi-threaded polyphase filterbank module for AMPP, which efficiently generates $2^{\rm n}$ spectral channels for each input subband. The number of output channels, the windowing function, the number of taps for the filter and the number of processing threads dedicated to the module are configurable options. In our searches so far, we use a filter that provides frequency channels with a bandwidth of 3.0518 kHz, by channelizing each incoming raw data subband into 64 channels. This increases the sample time from the original 5.12 μs to 327.68 μs.

Within the AMPP pipeline, the raw data are passed to a module which generates Stokes parameters from the incoming complex polarisations, according to:

$$\begin{aligned} I &= XX^* + YY^*, & Q &= XX^* - YY^* \\ U &= 2\mathrm{Re}(XY^*), & V &= -2\mathrm{Im}(XY^*), \end{aligned} \qquad (2)$$

where * refers to the complex conjugate. In the dispersion searches for FRBs described here, only Stokes-I (total power) is used. The software however provides the possibility to buffer all four Stokes parameters.

RFI is known to yield large numbers of false positives in pulsar searches (Eatough et al. 2009). The dedispersion transform integrates total power over frequency, thereby removing all frequency resolved information. This imposes the requirement to clean the data of RFI before dedispersion. Examples of RFI excision techniques for FRB searches have been described in Hogden et al. (2012). For our survey, removing RFI in real-time imposes specific constraints both on the algorithm (only information from the past data is available) and on the processing. The adaptive thresholding algorithm that we developed for AMPP performs the following steps:

(i) Prior to any observation, the spectral bandpass is recorded using narrow frequency channels. Individual bright channels are rejected through an iterative rejection process, and the clean bandpass is modelled using a low-order polynomial. The root mean square (RMS) of the bandpass noise is recorded.

(ii) The search commences.

(iii) Within AMPP, the total power data are processed by the RFI module one time sample at a time, consisting typically of a large number of spectral channels.

(iv) The median of each time sample spectrum is computed, which is insensitive to outliers, and the bandpass model is adjusted to that level (the zeroth order coefficient is set to the value of the spectrum mean).

(v) The power in each frequency channel is compared to the model at that frequency. If it exceeds a threshold $T_{\rm ch}$, it is given a small weight (in current implementations we set the weight to zero). $T_{\rm ch}$ is typically set to 6 times the RMS of the current bandpass noise.

(vi) The mean and RMS of this 'cleaned' spectrum are stored in a circular history buffer, which can hold values extended up to a duration much greater than the longest FRB searched for.

(vii) A running average of the history buffer is computed both for the model mean and the RMS, ensuring that the model remains up-to-date when it is compared to the next observed spectrum, without being affected by short term variability.

(viii) If the median value of the incoming spectrum reveals a large disagreement between the model and the spectrum, i.e., a jump has occurred in the incoming spectra due to a broadband signal, the whole spectrum is assigned a low weight. The threshold $T_{\rm sp}$ is typically also set to 6 times the calculated RMS of the median.

(ix) If the number of consecutive spectra that do not agree with the model is equal to the size of the history buffer, the algorithm accepts that the bandpass model is no longer relevant to the data, and sets the mean and RMS to the values of the last observed spectrum.

(x) Finally, for the FRB search, the bandpass model is removed from each flagged spectrum. AMPP has a configuration setting that allows each spectrum to be scaled to maintain a uniform RMS in the post-filtered data, which is very useful for the dedispersion transform.

Figure 2 shows the effect of the RFI excision algorithm on 1.3 s of filterbank data from the Rawlings Array. The algorithm described above effectively flags broadband signals

[1] `http://www.oerc.ox.ac.uk/~ska/pelican/`

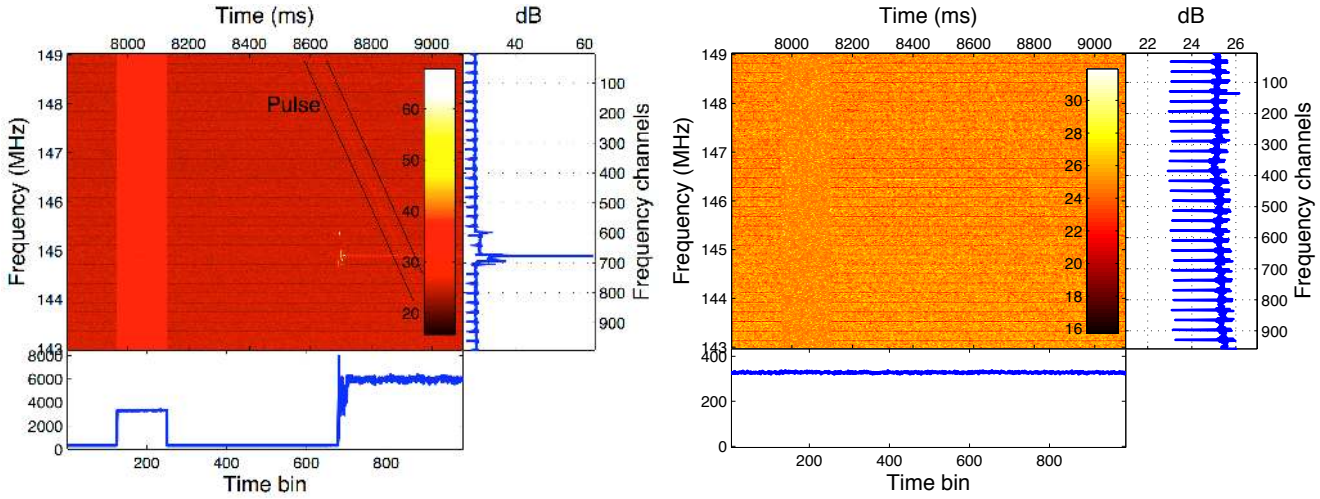

Figure 2. Filterbank data from the Rawlings Array. The central images show total power versus time and frequency. The bottom panel shows a time series of the total power integrated across frequency, and the panel to the right shows the bandpass averaged over time. In the bandpass, the series of parallel horizontal lines mark the boundaries of the LOFAR subbands, which have been further channelised in AMPP. The figure on the left shows data before the RFI excision module, including narrowband interference at ∼145 MHz which flares and sweeps across a narrow frequency range around time bin 680, and a broadband signal around time bin 200. The figure on the right shows the same data, post RFI filter. The broadband signal at time bin 200 has been flagged and in this case replaced by noise. The narrowband interference has been completely flagged out, revealing two dispersed bright pulses from PSR B0329+54, originally buried in the noise.

which raise the mean of the spectrum. In this example, the flagged data are replaced by Gaussian noise matching the bandpass model used for the comparison. However, for the real-time FRB searches, we set the weight of these data to zero, and replace them in the input to the dedispersion module with noise from a chi-squared distribution with four degrees of freedom. A narrowband (and in this case frequency-swept) signal of interference is also flagged, revealing two dispersed pulses of PSR B0329+54 in the processed filterbank data on the right. The RFI excision module can also be set to remove the mean of every spectrum, effectively removing signals at 0 DM (Eatough et al. 2009).

2.4 Dedispersion transform considerations

The dedispersion module used in AMPP was developed as part of the Astro-Accelerate library (Armour et al. 2012). This module performs the dedispersion transform between total power versus frequency and time, and total power versus dispersion measure and time. The software framework provides the infrastructure for setting up tasks on available GPUs, and GPU dedispersion kernels are used during AMPP processing. The details of the dedispersion process are beyond the scope of this paper and form the subject of a separate publication. Together with the RFI-cleaned data, the mean and standard deviation of the baseline noise are also propagated through the software pipeline to facilitate the detection of statistically significant signals in the de-dispersed data.

Incoherent dedispersion is performed in steps of DM. For technical reasons, pertaining to the dedispersion algorithm on a GPU, we maintain a fixed δDM step across the searched DM range. The dedispersion transform in our survey was therefore carried out at δDM steps of 0.1 cm^{-3} pc. This discretization results in some loss of signal due to intra-channel dispersion. Cordes & McLaughlin (2003) provide a framework for estimating the signal loss given the DM step size, the centre frequency and bandwidth of the observations and the width of a Gaussian pulse. Using their equations 12 and 13

$$\frac{S(\delta\mathrm{DM})}{S} = \frac{\sqrt{\pi}}{2}\zeta^{-1}\mathrm{erf}\zeta, \tag{3}$$

where

$$\zeta = 6.91 \times 10^{-3}\delta\mathrm{DM}\frac{\Delta\nu_{\mathrm{MHz}}}{W_{\mathrm{obs}}\nu^3_{\mathrm{GHz}}}. \tag{4}$$

and δDM = 0.1 cm^{-3} pc, we estimate a loss in sensitivity of less than 15% for 2 ms wide pulses, which drops to 2.5% for a 5 ms pulse.

Regardless of prior beliefs on the origin of FRBs, at a sky frequency of 145 MHz, interstellar scattering is a central consideration in the design of a search. Bhat et al. (2004) compute an empirical relationship between the measured scattering timescale τ and the DM of a large number of pulsars. There is at least an order of magnitude uncertainty in the DM-τ relationship. Scattering results in broadening of the intrinsic FRB width, resulting in a smaller loss of sensitivity, as per eqs. 3 and 4. To investigate relevant values of W_{obs} we assume the worst case scenario as regards dedispersion (i.e., the least possible scattering per given DM). We therefore set τ_{min} to be an order of magnitude smaller than what is given by Bhat et al. (2004). In principle, the observed width of a radio pulse is given by the convolution of τ_{min} with the intrinsic width of the burst, although for simplicity, we derive the observed width as

$$W^2_{\mathrm{obs}} = W^2_{\mathrm{int}} + \tau^2_{\mathrm{min}}, \tag{5}$$

where the intrinsic width W_{int} is defined in some reasonable way (e.g., FWHM). Another factor that comes into play

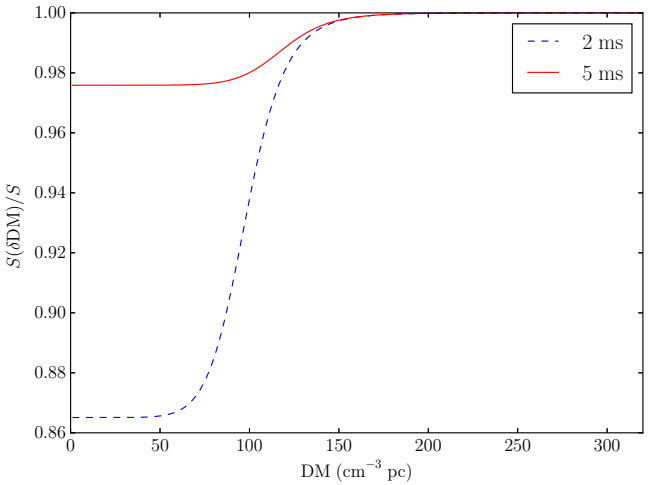

Figure 3. The efficiency $\frac{S(\delta\mathrm{DM})}{S}$ for a $\nu = 145$ MHz and $\Delta\nu = 6$ MHz search for FRBs with intrinsic width of 2 and 5 ms, given as a function of DM. The curve is computed using Eqs. 3, 4, 5, and setting τ_{min} to be 10% of what is given by Bhat et al. (2004). Regardless of the intrinsic FRB width, W_{obs} is likely dominated by the scattering timescale τ_{min} above a certain DM, thus rendering the efficiency high even for low intrinsic widths.

specifically for signals from cosmological distances is cosmological time dilation, which stretches the pulse by a factor of $(1 + z)$. However, as discussed in the following sections, z is small in the case of the ARTEMIS survey, so this effect can be safely neglected.

In the LOFAR HBA band at 145 MHz, there is a reasonable expectation that W_{obs} will be dominated by scattering above a certain DM. Figure 3 shows the efficiency $\frac{S(\delta\mathrm{DM})}{S}$ for a DM resolution δDM=0.1 cm^{-3} pc, for FRBs with an intrinsic width of 2 and 5 ms, based on the arguments above. The curves are characterised by a flat segment at the lowest DMs, which indicates the DM range for which Galactic scattering is unlikely to substantially broaden the pulse width ($W_{\mathrm{obs}} \approx W_{\mathrm{int}}$). The figure suggests that a DM resolution of $\delta DM = 0.1$ cm^{-3} pc maintains high efficiency even at low DM values.

Considering that FRBs typically last a few milliseconds sets an upper limit to the DM value searched using incoherent dedispersion. The reason is that intra-channel dispersion becomes large with increasing DM value at these low frequencies. Reducing the channel bandwidth is not an option, as it worsens the temporal resolution. For the channel bandwidth of 3.0518 kHz, the DM smearing at 145 MHz is 8.3μs per unit of DM. We have therefore chosen the maximum DM of our search to be 320 cm^{-3} pc, corresponding to a maximum of 2.6 ms of intra-channel smearing. To search for higher DM FRBs requires a step of coherent dedispersion, which would leave the temporal resolution unaffected.

The ARTEMIS hardware is capable of processing at least 3200 DM values per data stream in real-time, which is sufficient given the DM resolution arguments above. In fact, this sampling of the DM space was also chosen to demonstrate the viability of the hardware and software, operating at near maximum load. Dedispersed timeseries at neighbouring DM values will show some degree of correlation, however the threshold used for detection (10 times the noise RMS, see the following section), precludes spurious detections caused by this effect.

Once the filterbank data have been converted to a time series per DM, these are decimated to 2, 4, 8, 16, 32 and 64 times the original sampling time, and, along with the original, searched in real time for significant peaks by applying a 5-sample median filter to preclude the detection of single, high S/N peaks. We are currently investigating adaptive filtering algorithms for computational and detection performance.

3 FRB SEARCHES USING THE RAWLINGS ARRAY

We have currently concluded 1522 hours of drift-scan observations using the Rawlings Array. These observations were accompaniedfor the majority of the time by the French LOFAR international station at Nançay. The purpose of the second station was to perform a coincidence test on potential detected FRBs and rule out the possibility that they are caused by RFI.

The array is configured to point 8 beams with a bandwidth of 6.055 MHz (for odd-numbered beams) and 5.859 MHz (for even-numbered beams), to fixed positions in the sky on the local meridian, at declinations of 7.9°, 11°, 13.3°, 15.85°, 19°, 22°, 24.9°and 28.66°, corresponding to declinations of known bright pulsars which we use as sanity checks. Each beam is about 1.9°wide, and the total amount of instantaneous sky coverage is 24 sq. deg. Our sensitivity is given by

$$S_{\mathrm{min}} = 24.7 \text{ Jy} \left(\frac{10}{\sqrt{D}} \right), \qquad (6)$$

where 24.7 Jy is the noise RMS in each sample averaged across the band. This is computed by correcting the value given in Table 1, by the average elevation of our beams (58°). Furthermore, 10 is the threshold S/N ratio that we used, and D is the decimation factor, compared to the native 327.68 µs time resolution. This makes us sensitive to a peak flux density $\gtrsim 62$ Jy for 5 ms-duration pulses. This corresponds to a fluence, i.e. energy contained within a pulse, of 310 Jy ms. Note that, given the other decimation factors we have searched for, our survey has multiple fluence limits, ranging from 81 Jy ms for D=1 (pulse durations of 327µs) and 650 Jy ms for D=64 (pulse durations of 21 ms).

The survey searched for FRBs up to a DM of 320 cm^{-3} pc, covering a volume of 1.15×10^8 Mpc^3, which was computed in the following manner: Using the NE2001 model of electron density in the Galaxy (Cordes & Lazio 2002) and making the simple assumption that the potential host galaxy contributes a constant DM of 100 cm^{-3} pc, we can estimate the excess DM due to the IGM in each of our pointings. Figure 4 shows the pointings of the survey in Galactic coordinates. Pointings that did not probe outside the Galaxy (in the Galactic plane, indicated by red markers in Figure 4) were excluded from the volume calculation. Then, following Lorimer et al. (2007), we used the results of Ioka (2003) and Inoue (2004) to estimate the redshift corresponding to the IGM component of the DM. There are considerable uncertainties in the relationship between redshift and DM. Acknowledging this, we proceed by adopting DM=1200 z cm^{-3}

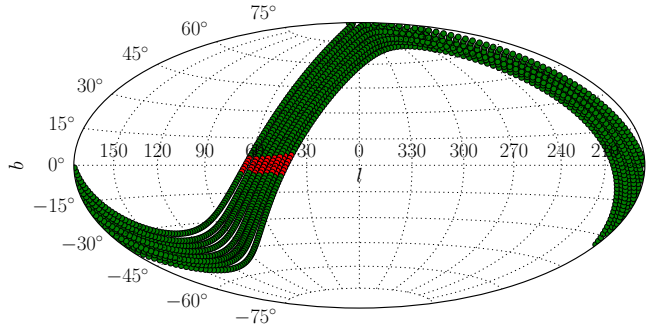

Figure 4. The pointings of the eight beams of the drift-scan survey. The red markers represent locations where the Galactic plane obscures extragalactic sources, while the green markers represent pointings that probed outside the Galaxy. The size and shape of the markers are not to scale.

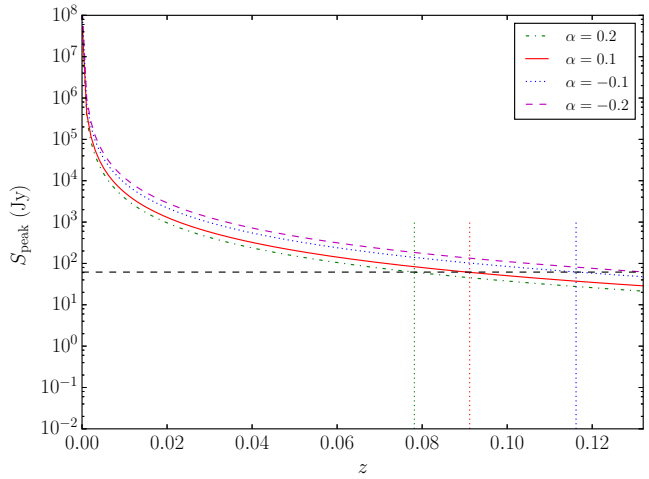

Figure 5. The relationship between the observed peak flux density for 5 ms-duration pulses and the source redshift, based on treating FRBs as standard candles (Lorimer et al. 2013), for various values of spectral index α. The black horizontal dashed line is the sensitivity limit of the ARTEMIS survey for 5 ms-duration bursts. The vertical lines are at the same redshifts as the vertical dotted lines in Figure 6, and help provide limits on the estimated spectral index of $\alpha = 0.1$, as described in detail in the text.

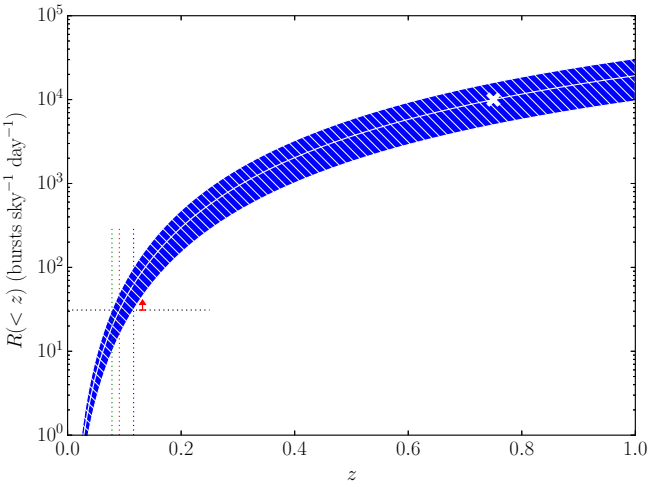

Figure 6. Reproduction of the centre panel of Figure 2 from Lorimer et al. (2013). The white cross is the Thornton et al. (2013) rate and the red arrow is the ARTEMIS upper limit. The white curve represents the FRB event rate at all redshifts constrained by the Thornton et al. (2013) rate, assuming that their survey was complete up to $z = 0.75$. The band around it represents the Poisson error on the Thornton et al. (2013) rate. The horizontal dotted line is at the level of the ARTEMIS upper limit, and intersects the extrapolated Thornton rate (and errors) at the vertical lines, which correspond to the redshift limits shown in Figure 5.

pc. Assuming a flat universe, we compute the comoving distance for each of the pointings, and the volume covered by the beam to that distance. The volumes corresponding to each extragalactic pointing are then summed to get the total volume. With the above assumptions, the maximum redshift probed in this survey was 0.17, and the average redshift among all our pointings is 0.13. We stress again the large associated uncertainties.

The average Galactic DM of all pointings that probed extragalactic space is 61.6 cm^{-3} pc, which, given our considerations about the host galaxy DM, justifies our DM spacing of 0.1 cm^{-3} pc (Figure 3). Given estimates of scatter-broadening related to these DM values in pulsars (Bhat et al. 2004), and comparatively small intergalactic scattering (Lorimer et al. 2013), we do not a priori expect scattering to render FRBs undetectable at the frequency and in the DM range of our survey.

Assuming FRBs are standard candles with broadband emission, the volume sampled by the survey may depend on their spectral index rather than the maximum DM. This can be understood as follows. Sources at a given maximum redshift should be bright enough at the frequency of observation to be detectable. Following Lorimer et al. (2013), we may be overestimating the volume in our survey if the spectral index of the sources is positive, as shown in Figure 5, where eq. 9 from Lorimer et al. (2013) is plotted for various values of spectral index. Figure 5 shows the relationship of the peak flux density of a 5 ms FRB as a function of redshift and spectral index. Lines of different spectral index – 0.2, 0.1, −0.1, −0.2 – are plotted. A horizontal line is placed at the sensitivity limit of the ARTEMIS survey. For a given maximum redshift, the minimum spectral index of detectable FRBs is the one that leads to a curve that intersects the sensitivity line at that redshift.

Figure 4 shows the sky coverage of the survey. Out of all the pointings in the survey, about 5% of pointings were limited to within the Galaxy due to the DM limit. We have excluded these pointings, leading to a total sky coverage in our survey of 4193 sq. deg. The total duration of the survey as it pertains to sensitivity towards extragalactic bursts reduces to 1446 hours. The single horizontal sensitivity line in Figure 5 is justified by the majority of our pointings being at high Galactic latitudes (>20°), where the sky temperature does not vary significantly.

3.1 Results

Our 1446-hour survey resulted in no detection of FRBs. Figure 7 shows an example of recorded events during the observing session of 19 September 2014. These consist of single pulses from known pulsars and sources of RFI. During the survey, the real-time processing software detected single pulses from all expected bright pulsars, including B0950+08, B1919+21, B1133+16, B0525+21, B0531+21 (the Crab pulsar), B2016+28, B2020+28, and B1237+25. This demonstrated the functionality of the system, including the ability to process a large number of DMs in real-time. We also serendipitously detected signals from HAMSAT, a low-Earth-orbit satellite whose signals appear at low, non-zero DMs. Despite the sophisticated adaptive RFI excision algorithm, a small number of spurious events were recorded per epoch, which were all evaluated by eye. For a 5 ms resolution, the total number of such events accounts for approximately 10^{-4} of the total searched parameter space in DM and time, and is therefore negligible in all calculations.

Based on the sky coverage and the time surveyed, and assuming an isotropic distribution of sources and completeness of the survey (for caveats, see Burke-Spolaor & Bannister 2014; Keane & Petroff 2015), we derive an upper limit to the rate of FRBs at 145 MHz, of 29 sky^{-1} day^{-1} for 5-ms-duration events above 62 Jy.

The non-detection of FRBs at low frequencies and their low numbers at 1.4 GHz makes inferring the nature of these sources difficult. Given the estimated survey volume, we could have observed FRBs from 1.15×10^6 host galaxies, assuming a galaxy density of 10^{-2} Mpc^{-3}. The amount of time however that each of these galaxies was covered by the survey beams is $\sim 10^{-3}$ yr, given the size and declination of the beams. Assuming the FRB volumetric rate in Thornton et al. (2013) of 10^{-3} Gal^{-1} yr^{-1}, that leaves us with a single potential FRB event in our survey. We therefore have to consider the possibility that no FRB occurred during the survey. Given the uncertainty in the relationship between DM and redshift, and given the uncertainty in the volumetric rates of FRBs at the present day, it is useful to consider other possible reasons for the non-detection, such as the spectral index of FRB emission.

As shown in Figure 5, where eq. 9 of Lorimer et al. (2013) is plotted for various values of the spectral index α, and as mentioned in the previous section, spectral index affects the volume surveyed. For values of α less than -0.2, the volume surveyed is dictated by the DM limit. For these values of α, following the standard candle model, we expect to see all bursts up to $z \approx 0.13$.

Figure 6 reproduces the centre panel of Figure 2 of Lorimer et al. (2013) up to $z = 1$, where the sky rate of bursts enclosed within a given volume is shown. The Thornton et al. (2013) rate is marked by the white cross. Our upper limit on the rate, of 29 bursts sky^{-1} day^{-1}, sits below the curve, and is marked by the red arrow. Assuming that FRBs occurred during our survey and given the caveats mentioned above, our null result could be explained by the most distant FRBs being too weak to observe, due to their spectrum. This leads to the realization that the maximum redshift is not set by DM considerations, but rather by the spectral index. To estimate the new maximum redshift, we observe that our sky rate is compatible with the Thornton et al. (2013) rate at a lower maximum redshift of $0.09^{+0.02}_{-0.01}$. This is the redshift at which the curve of the scaled Thornton rate of Figure 6 also becomes 29 sky^{-1} day^{-1}. Figure 5 allows us to associate a spectral index to the new maximum redshift probed, and errors on that spectral index based on the errors on the maximum redshift. Reading off Figure 5, this line of thinking allows us to place a lower limit on the spectral index of $0.1^{+0.1}_{-0.2}$.

We must point out that this line of reasoning also reduces the effective volume of the survey to 3.3×10^7 Mpc^3, leaving approximately one third of the host galaxies we started off with that could host an FRB. If, however, the true reason for our non-detection lies in the spectral properties rather than the volumetric rate, the implication is that the FRB spectral index is distinct from that of most pulsars. In the case of pulsars, a steep (negative) spectral index is thought to be indicative of a coherent emission process. The lack of such a steep spectrum in FRBs would serve as a clue to the nature of their emission process, which could be intrinsically more narrow-band than pulsars, or characterized by a frequency dependent emission geometry. It is worth noting that two of the published FRBs at this time have been observed to have a positive spectral index within the band of observation: a most likely value of α between 7 and 11, considering the frequency dependent telescope beam pattern, in Spitler et al. (2014), and 1.3 ± 1.6 in Ravi, Shannon, & Jameson (2015). Estimating spectral indices within an observing band is difficult due to effects of scintillation and frequency dependent gain variation within the telescope beam. This latter effect is more likely to render the observed spectrum to have a more negative slope than its intrinsic slope. Therefore, despite the small population of FRBs with a positive spectral index, a consistent picture may be emerging.

In estimating the FRB spectral index from our survey we have assumed that FRBs are extragalactic standard candles with broadband radio emission. We have also implicitly assumed that the volumetric rate of FRBs, that reflects the rate per galaxy per year, is constant with redshift. We have not tested the standard candle hypothesis, while the volumetric rate may be a function of redshift, similar to the redshift dependent star formation rate.

4 DISCUSSION AND CONCLUSIONS

We have developed ARTEMIS, a GPU-based real-time fast transient detection system that works with individual LOFAR stations. We have used the deployment at the Rawlings Array to demonstrate the functionality and performance of the system using known pulsars. We conducted a 1446 hour drift-scan survey for FRBs, searching the DM space up to 320 cm^{-3} pc. With a series of arguments relating to sensitivity and the intrinsic spectra of FRBs, and some simple assumptions about their nature, we estimate that we have surveyed a volume of 3.3×10^7 Mpc^3.

No FRB was detected in the survey at the Rawlings Array or indeed the Nançay station, and we derive an upper limit of 29 FRBs sky^{-1} day^{-1} within the parameters of our search. The non-detection could be due to one or more of the following reasons: Not enough volume surveyed for enough time, interstellar and intergalactic scattering, and the intrinsic spectra of FRBs.

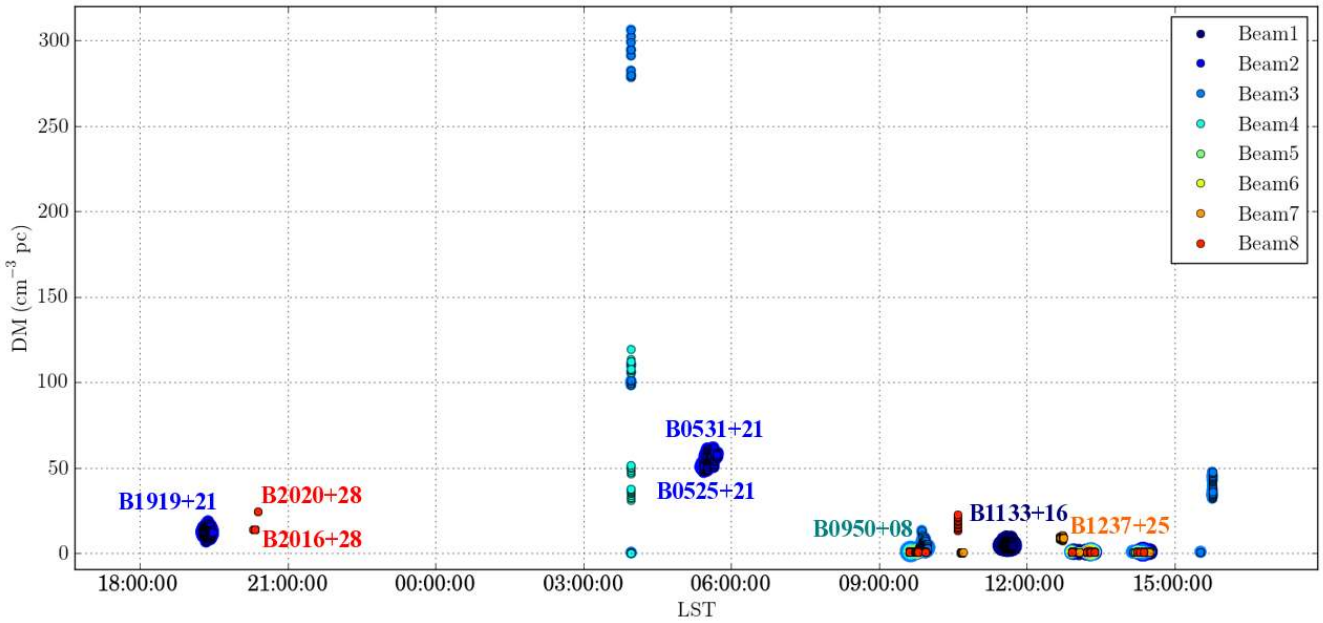

Figure 7. A sample output plot of single pulse detections in the ARTEMIS survey, showing a few pulsars and some RFI. Each cluster of markers correspond to single pulses from a pulsar, while the sets of points, elongated in DM, are RFI.

Assuming the latter, we have attempted to constrain the spectral index of FRBs, to $\alpha \gtrsim 0.1^{+0.1}_{-0.2}$, assuming a standard candle model. The physical significance of this result is moderated by the fact that we cannot rule out other causes of non-detection at the frequency of our survey, including the possibility that FRBs are local events to the telescopes that have detected them. Assuming that the non-detection is indeed due to the intrinsic shape of FRB spectra, our result is constrained by the sensitivity of the Rawlings Array.

This work has implications for future low frequency FRB surveys. Firstly, at frequencies around 145 MHz, longer duration surveys with increased telescope sensitivity could allow further constraints of the spectral index to even higher values, or detect FRBs. It is however quite difficult to sample substantially more volume of Universe, without running into greater potential scattering effects. Secondly, moving up in frequency by a factor of 2 and increasing the sensitivity by two orders of magnitude, which will ultimately be interesting for the low frequency component of the Square Kilometre Array, could allow surveys to probe redshifts upwards of z=1. Assuming scatter broadening is mainly due to propagation in the host galaxy and our galaxy, there is a reasonable expectation that it will not affect these predictions. This suggests that future high-sensitivity surveys at 300 MHz, should result in a reasonable yield of new FRBs and should resolve the spectral index question.

For ARTEMIS, we are developing a commensal real-time system in collaboration with the Berkeley SETI Research Center, for the Arecibo radio telescope. Named ALFABURST, this system will use the seven-beam L-band feed of the Arecibo telescope to perform surveys for FRBs, potentially increasing the sample size. In this system, we aim to incorporate multi-beam coincidence rejection that will reduce the number of false alarms, and automated triggering that will alert low-frequency telescopes in the event that an FRB is detected. Similar systems are being prepared for the South African SKA pathfinders (KAT-7 and MeerKAT) and for tied-array beams of the LOFAR International Telescope that offer an order of magnitude improvement in sensitivity.

ACKNOWLEDGMENTS

We would like to thank Dr Alex Kraus and staff at the Effelsberg Radiotelescope for hosting us and our machines during early ARTEMIS development. AK, WA and JC would like to thank the Leverhulme Trust for supporting this work. The Rawlings Array is operated by LOFAR-UK as part of the International LOFAR Telescope, and is funded by LOFAR-UK and STFC. SO is supported by the Alexander von Humboldt Foundation.

REFERENCES

Armour W., et al., 2012, in Ballester P., Egret D., Lorente N. P. F., eds, Astronomical Data Analysis Software and Systems XXI Vol. 461 of Astronomical Society of the Pacific Conference Series, A GPU-based Survey for Millisecond Radio Transients Using ARTEMIS. p. 33
Bannister K. W., Madsen G. J., 2014, MNRAS, 440, 353
Barsdell B. R., Bailes M., Barnes D. G., Fluke C. J., 2012, MNRAS, 422, 379
Bhat N. D. R., Cordes J. M., Camilo F., Nice D. J., Lorimer D. R., 2004, ApJ, 605, 759
Burke-Spolaor S., Bannister K. W., 2014, ApJ, 792, 19
Coenen T., et al., 2014, A&A, 570, A60
Cordes J. M., Lazio T. J. W., 2002, astro-ph/0207156
Cordes J. M., McLaughlin M. A., 2003, ApJ, 596, 1142
Eatough R. P., Keane E. F., Lyne A. G., 2009, MNRAS, 395, 410
Falcke H., Rezzolla L., 2014, A&A, 562, A137

Hogden J., Vander Wiel S., Bower G. C., Michalak S., Siemion A., Werthimer D., 2012, ApJ, 747, 141
Inoue S., 2004, MNRAS, 348, 999
Ioka K., 2003, ApJ, 598, L79
Keane E. F., Petroff E., 2015, MNRAS, 447, 2852
Keane E. F., Stappers B. W., Kramer M., Lyne A. G., 2012, MNRAS, 425, L71
Keith M. J., et al., 2010, MNRAS, 409, 619
Loeb A., Shvartzvald Y., Maoz D., 2014, MNRAS, 439, L46
Lorimer D. R., Bailes M., McLaughlin M. A., Narkevic D. J., Crawford F., 2007, Science, 318, 777
Lorimer D. R., Karastergiou A., McLaughlin M. A., Johnston S., 2013, MNRAS, 436, L5
Lorimer D. R., Kramer M., 2004, Handbook of pulsar astronomy. Cambridge observing handbooks for research astronomers, Vol. 4. Cambridge, UK: Cambridge University Press, 2004
Macquart J.-P., et al., 2015, arXiv, arXiv:1501.07535
Magro A., Karastergiou A., Salvini S., Mort B., Dulwich F., Zarb Adami K., 2011, MNRAS, 417, 2642
McLaughlin M. A., Cordes J. M., 2003, ApJ, 596, 982
McLaughlin M. A., et al., 2006, Nature, 439, 817
McQuinn M., 2014, ApJ, 780, L33
Mol J. D., Romein J. W., 2011, ArXiv e-prints
Mottez F., Zarka P., 2014, A&A, 569, A86
Persic M., Salucci P., 1992, MNRAS, 258, 14P
Petroff E., et al., 2015, MNRAS, 447, 246
Popov S. B., Postnov K. A., 2013, ArXiv e-prints
Ravi V., Shannon R. M., Jameson A., 2015, ApJ, 799, LL5
Spitler L. G., et al., 2014, ApJ, 790, 101
Stappers B. W., et al., 2011, A&A, 530, A80
Thornton D., et al., 2013, Science, 341, 53
Totani T., 2013, PASJ, 65, L12
Trott C. M., Tingay S. J., Wayth R. B., 2013, ApJ, 776, L16
van Haarlem M. P., et al., 2013, A&A, 556, A2
Wayth R. B., Tingay S. J., Deller A. T., Brisken W. F., Thompson D. R., Wagstaff K. L., Majid W. A., 2012, ApJ, 753, L36